Topographic Forcing of Coastal Mesoscale Phenomena: Filamentation, Vortex Formation, and Eddy Detachment

FERNANDO VIERA

School of Mathematics and Statistics, The University of Sydney, New South Wales, Australia

ROGER GRIMSHAW

Department of Mathematics, Monash University, Clayton, Victoria, Australia

(Manuscript received 10 February 1993, in final form 17 August 1993)

ABSTRACT

Using the methodology of contour dynamics on a quasigeostrophic model, the nonlinear evolution of a coastal potential vorticity front over a Gaussian topographic feature in the presence of an overlying linearly stable basic flow is investigated. The simulations show that increasing the amplitude of the forcing leads to four different qualitative regimes: 1) small amplitude wavelike disturbances are formed, 2) a primary (trapped) disturbance breaks and forms filaments, 3) a secondary (moving) disturbance breaks and forms filaments, and 4) the primary filament winds around the topographic feature until an eddy with considerable internal mixing finally detaches. Other parameters such as the topographic width, the position of the undisturbed front relative to the topography, and the potential vorticity in the ocean region are also shown to be important in controlling (either enhancing or inhibiting) the process of filamentation and vortex formation. The main conclusion is that nonlinear dynamics alone may be responsible for the formation of meanders and eddies without the necessary presence of instabilities in the basic flow.

1. Introduction

New advances in remote sensing techniques and the ability to obtain high quality datasets have revealed the presence of oceanic mesoscale phenomena of spatial scales of the order of 100 km in coastal waters in many parts of the world. Observations of meanders and mesoscale eddies by Griffiths and Pearce (1985), Huyer and Kosro (1987), and Kosro (1987) have emphasized the importance of both topographic forcing and instabilities in the formation and evolution of such phenomena. Observation of filaments off the west coast of the United States is well documented by Brink and Cowles (1991). Haidvogel et al. (1991) have carried out numerical simulations of the formation and evolution of filaments for a baroclinic ocean in the coastal transition zone, and Narimousa and Maxworthy (1989) conducted numerous laboratory studies of coastal ocean jet flows over topography. It is clear from these studies that steady flows over large amplitude topography will produce a rich variety of transient behavior such as meandering, filamenting jets, and isolated eddies.

On the theoretical side, the study of the fully nonlinear evolution of waves on a vorticity front using the method of contour dynamics has provided some insight into the processes leading to eddy formation and detachment (e.g., Pratt and Stern 1986). In particular, the effects of barotropic instabilities of waves on oceanic fronts have been studied in some detail by Send (1989) and Pratt and Pedlosky (1991). Little is known, however, of the effects of topographic forcing on the nonlinear evolution of a vorticity front with a linearly stable basic flow. Grimshaw and Yi (1991, 1992) studied the evolution of initial disturbances on a potential vorticity front over a topographic slope with a stable basic flow and found that even small amplitude disturbances may evolve as long filaments. They also found that very steep topographic slopes have a tendency to enhance eddy formation at the tip of a vorticity filament. They concluded that it is not always necessary to have an underlying linear instability to obtain the filamentation required for subsequent eddy formation and detachment.

Motivated by the results of the aforementioned studies, in this paper we investigate the evolution of a potential vorticity front over an isolated topographic feature and identify conditions for which filamentation and eddy formation are possible on a linearly stable basic flow. Using a quasigeostrophic model, we follow Pratt and Stern (1986) and formulate a contour dy-

Corresponding author address: Dr. Fernando Viera, School of Mathematics and Statistics, The University of Sydney, NSW 2006, Australia.

e-mail: viera_f@maths.su.oz.au

namics algorithm for the evolution of waves that form at a vorticity interface separating two regions of constant potential vorticities Q_0 and Q_1. A Gaussian topographic feature is switched on at $t = 0$ and acts as a source of potential vorticity. Since the basic flow is stable, the initial transients generated by the turning on of the topography instantaneously at $t = 0$ are small and propagate away quickly.

The principal aim is to determine the parameter values of the topographic forcing and the basic flow that lead to filamentation and vortex formation. In section 2 we formulate the problem. In section 3 we develop the contour dynamical equations and the numerical algorithm. In section 4 we present the results of the simulations and a summary is given in section 5.

2. Problem formulation

We consider a quasigeostrophic model consisting of a single density layer of mean depth D below a deep inactive layer. The motion of the lower layer is then equivalent to the motion of a single layer under reduced gravity g'. Let d be a typical depth variation of the undisturbed surface so that the Rossby number $\mathrm{Ro} = d/D \ll 1$ and choose the Rossby radius of deformation $(g'D)^{1/2}/f$ as the horizontal length scale, where f is the Coriolis parameter. If time is nondimensionalized by $(fd/D)^{-1}$ and potential vorticity by fd/D^2, then the conservation of quasigeostrophic potential vorticity Q following fluid particles with velocity (u, v) is

$$Q_t + uQ_x + vQ_y = 0, \tag{2.1a}$$

where

$$Q = \nabla^2\psi - \psi + h(x, y). \tag{2.1b}$$

Here $\psi(x, y, t)$ is the streamfunction of (u, v), such that

$$u = -\psi_y, \quad v = \psi_x, \tag{2.1c}$$

and

$$\mathrm{Ro}h(x, y) \ll 1$$

is the nondimensional bottom topography measured upward. For example, typical Rossby numbers for mesoscale phenomena are $O(10^{-3})$. Note that even if the maximum height of $h(x, y)$ in this nondimensional coordinate system is allowed to be as large as 10, the actual height of the topography is quite small and quasigeostrophic dynamics still applies. Since we are interested in the effects of an isolated topographic feature, we assume that $h(x, y) \to 0$ as $x^2 + y^2 \to \infty$. The boundary conditions are that

$$\psi_y = 0, \quad \text{at} \quad x = 0 \tag{2.2a}$$

and

$$\psi_y \to 0, \quad \text{as} \quad x \to \infty, \tag{2.2b}$$

which are the conditions for zero flow in the on–offshore direction at the coast, and in the distant ocean, respectively.

Now let $x = L(y, t)$ denote the position of a potential vorticity interface with undisturbed position $x = l$, and assume that

$$Q = \begin{cases} Q_0, & \text{for} \quad x > L \\ Q_1, & \text{for} \quad 0 < x < L, \end{cases} \tag{2.3}$$

where Q_0 and Q_1 are the constant values of the potential vorticity on either side of the interface (Fig. 1). It is convenient to separate the flow into a basic state with streamfunction $\psi_0(x)$ plus a perturbation streamfunction $\phi(x, y, t)$, so that

$$\psi(x, y, t) = \psi_0(x) + \phi(x, y, t), \tag{2.4}$$

with corresponding velocity field

$$u(x, y, t) = -\phi_y(x, y, t), \tag{2.5a}$$

$$v(x, y, t) = v_0(x) + \phi_x(x, y, t). \tag{2.5b}$$

The equation for $\psi_0(x)$ is obtained by taking the limit $y \to -\infty$ in (2.1b) and assuming that $L \to l$ and $\phi \to 0$ in this limit so that

$$\psi_{0xx} - \psi_0 = \begin{cases} Q_0, & \text{for} \quad x > l \\ Q_1, & \text{for} \quad 0 < x < l. \end{cases} \tag{2.6}$$

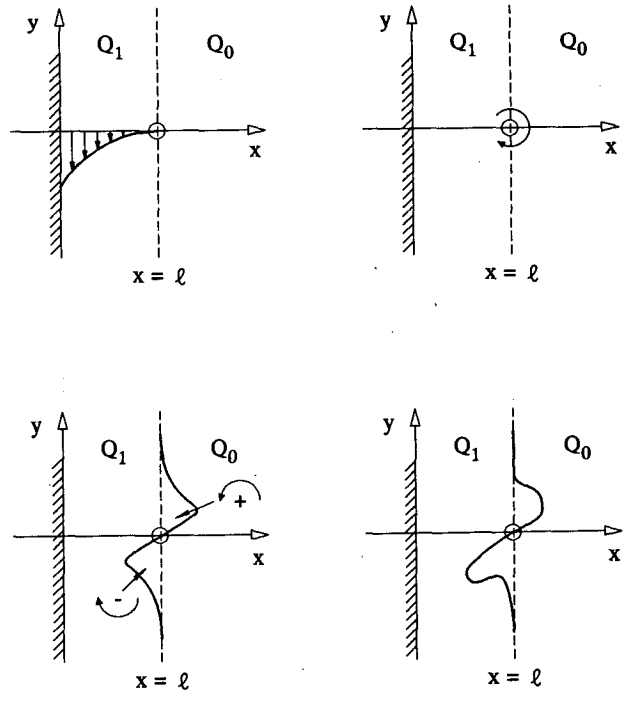

FIG. 1. (a) The coordinate system, the undisturbed position of the vorticity interface $x = l$, and the basic flow for $Q_0 = 0$, $\Delta Q = 1$, and $h_0 > 0$. (b) The negative relative vorticity induced by the topographic feature. (c) The relative vorticity anomalies induced by the vorticity jump ΔQ. (d) Advection of the disturbance by the basic flow.

The solution of (2.6) that is finite as $x \to \infty$ gives the linearly stable basic flow

$$v_0(x) = \begin{cases} -Be^{-(x-l)}, & x > l \\ -Be^{-(x-l)} + (Q_1 - Q_0)\sinh(x-l), & 0 < x < l, \end{cases} \quad (2.7a)$$

where B is an arbitrary constant. In what follows we set $B = Q_0$, giving $\psi_0 = 0$ at $x = l$. However, we note that ψ_0 is also the height of the free surface and in general if $\psi_0 = D_0$ at $x = l$ then $B = Q_0 + D_0$. This gives

$$v_0(x) = \begin{cases} -\hat{Q}_0 e^{-(x-l)}, & x > l \\ -\hat{Q}_0 e^{-(x-l)} + (\hat{Q}_1 - \hat{Q}_0)\sinh(x-l), & 0 < x < l, \end{cases} \quad (2.7b)$$

where $\hat{Q}_0 = Q_0 + D_0$, $\hat{Q}_1 = Q_1 + D_0$. That is, changing D_0 is equivalent to changing Q_0 and Q_1 by the same amount, and leaving the difference unchanged.

Substituting (2.4) into (2.1b) and using (2.3) we find an equation for the perturbation streamfunction,

$$\nabla^2\phi - \phi = \Phi(x, y, t) - h(x, y), \quad (2.8a)$$

where

$$\Phi(x, y, t) = \begin{cases} \Delta Q, & l < x < L \\ -\Delta Q, & L < x < l \\ 0, & \text{otherwise,} \end{cases} \quad (2.8b)$$

and $\Delta Q = Q_1 - Q_0$. The boundary conditions are that

$$\phi = 0 \quad \text{at} \quad x = 0, \quad (2.9a)$$

$$\phi \to 0 \quad \text{as} \quad x^2 + y^2 \to \infty, \quad (2.9b)$$

and ϕ, ϕ_x, and ϕ_y are continuous across the front $x = L(y, t)$.

A formal solution of (2.8) that satisfies the boundary conditions (2.9) can be constructed using the Green's function of the Helmholtz operator $\nabla^2 - 1$,

$$G(x, x', y, y') = -\frac{1}{2\pi} K_0(R), \quad (2.10a)$$

where

$$R = [(x - x')^2 + (y - y')^2]^{1/2}, \quad (2.10b)$$

and $K_0(R)$ is the modified Bessel function of the second kind. Using Green's integral identities, we find the solution

$$\phi(x, y, t) = \Delta Q \int_{-\infty}^{\infty} \int_{l}^{L(y',t)} [G(R) - G(R_I)]dx'dy' - \int_{-\infty}^{\infty} \int_{-\infty}^{\infty} h(x', y')[G(R) - G(R_I)]dx'dy', \quad (2.11a)$$

where

$$R_I = [(x + x')^2 + (y - y')^2]^{1/2}, \quad (2.11b)$$

and $G(R_I)$ is an image term that has been introduced to satisfy the coastal boundary condition (2.9a). The first term in (2.11) is the contribution from the potential vorticity jump (the vorticity anomaly), while the second integral is the term corresponding to the topographic forcing.

3. Contour dynamics algorithm

To develop the contour dynamics formulation we follow each point (L, y) on the vorticity interface according to the Lagrangian equations

$$\frac{dL}{dt} = u(L, y, t), \quad \frac{dy}{dt} = v(L, y, t), \quad (3.1)$$

where the velocity field (u, v) obtained from (2.5) is

$$u(x, y, t) = J_1 + A_1, \quad (3.2a)$$

$$v(x, y, t) - v_0(x) = J_2 + A_2, \quad (3.2b)$$

where

$$J_1(x, y, t) = -\Delta Q \frac{\partial}{\partial y} \int_{-\infty}^{\infty} dy' \times \int_{l}^{L(y',t)} [G(R) - G(R_I)]dx' \quad (3.3a)$$

$$J_2(x, y, t) = \Delta Q \frac{\partial}{\partial x} \int_{-\infty}^{\infty} dy' \times \int_{l}^{L(y',t)} [G(R) - G(R_I)]dx' \quad (3.3b)$$

$$A_1(x, y) = \int_{-\infty}^{\infty} \int_{-\infty}^{\infty} h(x', y') \times \frac{\partial}{\partial y}[G(R) - G(R_I)]dx'dy' \quad (3.4a)$$

$$A_2(x, y) = -\int_{-\infty}^{\infty} \int_{-\infty}^{\infty} h(x', y') \times \frac{\partial}{\partial x}[G(R) - G(R_I)]dx'dy'. \quad (3.4b)$$

The integrals over the area of the displaced contour, J_1 and J_2, are transformed into integrals along the contour by integrating by parts to obtain

$$J_1(x, y, t) = -\Delta Q \int_{-\infty}^{\infty} [G(x, L', y, y') - G(x, -L', y, y')]dL' \quad (3.5a)$$

$$J_2(x, y, t) = -\Delta Q \int_{-\infty}^{\infty} [G(x, L', y, y') + G(x, -L', y, y')]dy' + \Delta Q \int_{-\infty}^{\infty} [G(x, l, y, y') + G(x, -l, y, y')]dy', \quad (3.5b)$$

where

$$L' = L(y', t), \quad dL' = \frac{\partial L}{\partial y'} dy'. \quad (3.5c)$$

Next we calculate the forcing terms given by the area integrals (3.4) assuming the bottom topography $h(x, y)$ is given by a Gaussian function of the form

$$h(x, y) = h_0 \exp\{-\xi[(x - \bar{x}_0)^2 + (y - \bar{y}_0)^2]\}. \quad (3.6)$$

This represents an isolated topographic feature centered at the point $(\bar{x}_0, \bar{y}_0)$, of amplitude h_0 and half-width $\xi^{-1/2}$. We show in appendix A that the double integrals (3.4) may be reduced to single integrals with the result that

$$A_1(x, y) = -h_0 \int_0^{\infty} e^{-\xi\lambda^2} K_1(\lambda)[-B_1(x, y, \lambda) + B_1(-x, y, \lambda)]\lambda d\lambda \quad (3.7a)$$

$$A_2(x, y) = -h_0 \int_0^{\infty} e^{-\xi\lambda^2} K_1(\lambda)[B_2(x, y, \lambda) + B_2(-x, y, \lambda)]\lambda d\lambda, \quad (3.7b)$$

where

$$B_1(x, y, \lambda) = \frac{(y - \bar{y}_0)}{A} e^{-\xi A^2} I_1(2\xi A\lambda) \quad (3.7c)$$

$$B_2(x, y, \lambda) = \frac{(x - \bar{x}_0)}{(y - \bar{y}_0)} B_1(x, y, \lambda) \quad (3.7d)$$

$$A^2 = (x - \bar{x}_0)^2 + (y - \bar{y}_0)^2,$$

and $I_1(\lambda)$ and $K_1(\lambda)$ are the modified Bessel functions of order one. We note that the integrands in (3.7) decay exponentially and therefore the integrals can be calculated using Simpson's rule and truncating the upper limit to a suitable value. Finally, substituting (3.2) into (3.1) with (3.5) and (3.7) gives the integro–differential equations for the contour dynamics calculation of the evolution of the interface $L(y, t)$.

Next, we discretize the contour with N points $[L_i(t), y_i(t)]$, for $i = 1, \cdots, N$, and consequently we obtain the discretized version of (3.1); namely,

$$\frac{dL_i}{dt} = u(L_i, y_i, t),$$

$$\frac{dy_i}{dt} = v(L_i, y_i, t), \quad \text{for} \quad i = 1, \cdots, N. \quad (3.8)$$

We introduce the fixed points (y_0, L_0) and (y_{N+1}, L_{N+1}) where $L_0 = L_{N+1} = l$ and assume that the contour is not displaced for $y \leqslant y_0$ and $y \geqslant y_{N+1}$. The integrals J_1 and J_2 in (3.5) are approximated by the trapezoidal rule as follows:

$$J_1(L_i, y_i) = -\tfrac{1}{2}\Delta Q\{(L_1 - L_0)[G(R'_{i0}) - G(R'_{Ii0})] + (L_{N+1} - L_N)[G(R'_{iN+1}) - G(R'_{IiN+1})]\} - \tfrac{1}{2}\Delta Q \sum_{j=1}^{N}{}' (L_{j+1} - L_{j-1})[G(R'_{ij}) - G(R'_{Iij})] - \Delta Q \int_{L_{i-1}}^{L_{i+1}} G(R'_i)dL', \quad (3.9)$$

where

$$R'_{ij} = [(L_i - L_j)^2 + (y_i - y_j)^2]^{1/2} \quad (3.10a)$$

$$R'_{Iij} = [(L_i + L_j)^2 + (y_i - y_j)^2]^{1/2} \quad (3.10b)$$

$$R'_i = [(L_i - L')^2 + (y_i - y')^2]^{1/2}. \quad (3.10c)$$

In the above, Σ' denotes the sum where for $i = j$, the term $(L_{j+1} - L_{j-1})G(R'_{ij})$ has been omitted.

The last term in (3.9) is a singular integral and we treat it in a similar way to Jacobs and Pullin (1989) and Grimshaw and Yi (1991). Essentially, the curve is approximated by the parabola

$$L' = L_i + \tfrac{1}{2}(L_{i+1} - L_{i-1})e + \tfrac{1}{2}(L_{i+1} + L_{i-1} - 2L_i)e^2 \quad (3.11a)$$

$$y' = y_i + \tfrac{1}{2}(y_{i+1} - y_{i-1})e + \tfrac{1}{2}(y_{i+1} + y_{i-1} - 2y_i)e^2, \quad (3.11b)$$

where $-1 \leqslant e \leqslant 1$. The logarithmic singularity is extracted from $G(R)$ using the asymptotic formula

$$K_0(R) \sim -\ln R - \gamma, \quad \text{as} \quad R \to 0, \quad (3.12)$$

where γ is Euler's constant. The integration is then done analytically with the result that

$$\int_{L_{i-1}}^{L_{i+1}} G(R_i')dL' = \int_{-1}^{1} \left[\frac{dL'}{de} G(R_i') - \alpha_i \ln|e|\right]de - 2\alpha_i, \quad (3.13a)$$

where

$$\alpha_i = \frac{1}{2\pi}\frac{dL'}{de}\bigg|_{e=0} = \frac{1}{4\pi}(L_{i+1} - L_{i-1}). \quad (3.13b)$$

The integral in (3.13a) is finally evaluated by Simpson's rule.

Similarly, the two integrals in (3.5b) become

$$J_2(L_i, y_i) = -\frac{1}{2}\Delta Q \sum_{j=1}^{N}{}' (y_{j+1} - y_{j-1})[G(R'_{ij}) + G(R'_{Iij})] - \Delta Q \int_{y_{i-1}}^{y_{i+1}} G(R_i')dy' + \frac{1}{2}\Delta Q \sum_{j=1}^{N} (y_{j+1} - y_{j-1})[G(R'_{Iij}) + G(R'_{IIij})], \quad (3.14a)$$

where there is a cancellation between the end terms of the trapezoidal approximation and the corresponding terms of the tail integrals. Here,

$$R'_{Iij} = [(L_i - l)^2 + (y_i - y_j)^2]^{1/2} \quad (3.14b)$$

$$R'_{IIij} = [(L_i + l)^2 + (y_i - y_j)^2]^{1/2}. \quad (3.14c)$$

The singular integral in (3.14a) is treated as in (3.9) with the result that

$$\int_{y_{i-1}}^{y_{i+1}} G(R_i')dy' = \int_{-1}^{1} \left[\frac{dy'}{de} G(R_i') - \beta_i \ln|e|\right]de - 2\beta_i, \quad (3.15a)$$

where

$$\beta_i = \frac{1}{2\pi}\frac{dy'}{de}\bigg|_{e=0} = \frac{1}{4\pi}(y_{i+1} - y_{i-1}). \quad (3.15b)$$

Although in this problem we do not use the more sophisticated algorithms of contour surgery (e.g., Dritschel 1989), the points at the interface are rearranged after each time step using the insertion/deletion algorithm of Pullin and Jacobs (1986). This is necessary in order to maintain adequate resolution throughout the integration because the density of points along the contour tends to increase in regions of high curvature and decrease in sections of low curvature. The time stepping is performed using a standard fourth-order Runge–Kutta method.

4. Numerical results

Before proceeding to describe our numerical results, we perform a qualitative potential vorticity analysis in order to predict the initial evolution of the front. Suppose the topography is centered at the point $(\bar{x}_0, \bar{y}_0) = (1, 0)$ (indicated by a small circle in Fig. 1), and let $l = 1$. We then take the initial position of the front to be the straight line $L(y, 0) = 1$. This means that the center of the topographic feature coincides with the undisturbed position of the front. Suppose also that $Q_0 = 0$, $\Delta Q = 1$, and $h_0 > 0$. The basic flow then advects fluid in the negative y direction for $x < l$ as shown in Fig. 1a. Since $h > 0$, Eq. (2.8a) shows that the induced perturbation potential vorticity $\nabla^2\phi - \phi < 0$, while (2.11a) shows that $\phi > 0$ (since $G < 0$ and $|G(R_I)|$ is much smaller than $|G(R)|$). Thus, the induced relative vorticity $\nabla^2\phi$ is negative over the topography, and hence the front will tend to be displaced in the manner indicated in Fig. 1c, that is, a positive vorticity anomaly for $l < x < L$ and a negative vorticity anomaly for $L < x < l$. The displacements induced by these latter relative vorticity anomalies correspond to a phase propagation in the negative y direction. Finally, when the basic flow is included, the section of the front in $x < l$ will be advected in the negative y direction as shown in Fig. 1d. Similar analyses can be carried out for other sign combinations of h_0, ΔQ, and for basic flows with $Q_0 \neq 0$.

The available parameters are h_0, ξ for the height and width of the bottom topography, $(\bar{x}_0, \bar{y}_0)$ for the location of the bottom topography, Q_0 and $\Delta Q = Q_1 - Q_0$ for the potential vorticity distribution, and l for the upstream location of the potential vorticity front. Of these $|\Delta Q|$ can be absorbed into the time scale, and sign ΔQ can be linked to sign y. Hence there is no loss of generality in setting $\Delta Q = 1$. For the topographic parameters we can set $\bar{y}_0 = 0$ without loss of generality, leaving the height h_0, the width $\xi^{-1/2}$, and the distance from the coast $\bar{x}_0$ as the parameters to be varied. With $\Delta Q = 1$, we can vary Q_0, the basic state potential vorticity in $x > L$, and l, the upstream location of the potential vorticity front. Further parameters could be introduced by the initial conditions, but here we set $L = l$ at $t = 0$. In effect the topography is

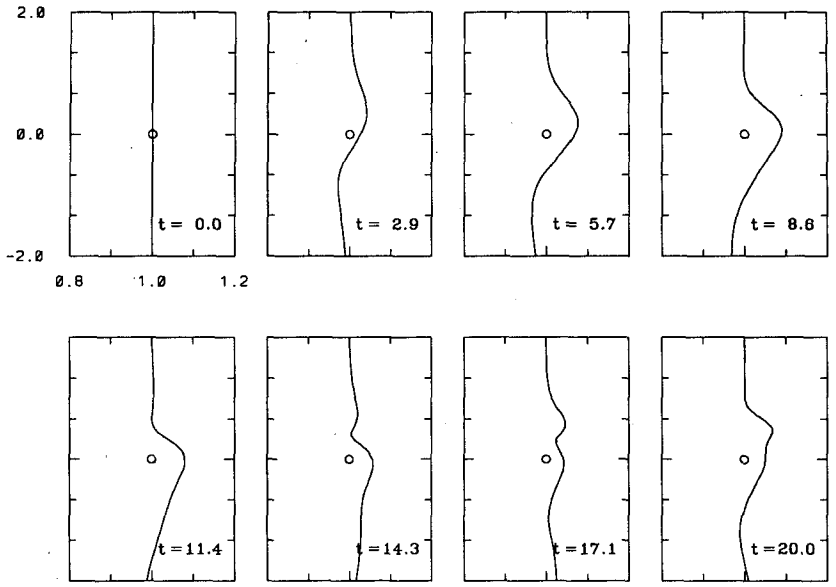

FIG. 2a. The evolution of the front for $Q_0 = 0$, $\Delta Q = 1$, $\xi = 3$, $l = 1$, and $h_0 = 0.1$.

turned on at $t = 0$. The end points of the contour are always taken sufficiently far from the topography so that they remain fixed over the period of integration. In a typical run we start with 200 nodal points and let the number increase to about 800 points at the end of the integration interval. The area of the displaced contour,

$$A = \int_{-\infty}^{\infty} \int_{l}^{L(y,t)} dx'dy', \tag{4.1}$$

is a constant and is used to provide a check on the numerical calculations.

a. *Varying* h_0

We now take $\xi = 3$ for numerical convenience and, fixing all other parameters as in Fig. 1, we vary the topographic amplitude h_0. Figure 2a shows the evolution of the front for $h_0 = 0.1$. The box corresponding to $t = 2.9$ shows that the initial stage of evolution is consistent with the previous potential vorticity analysis. The

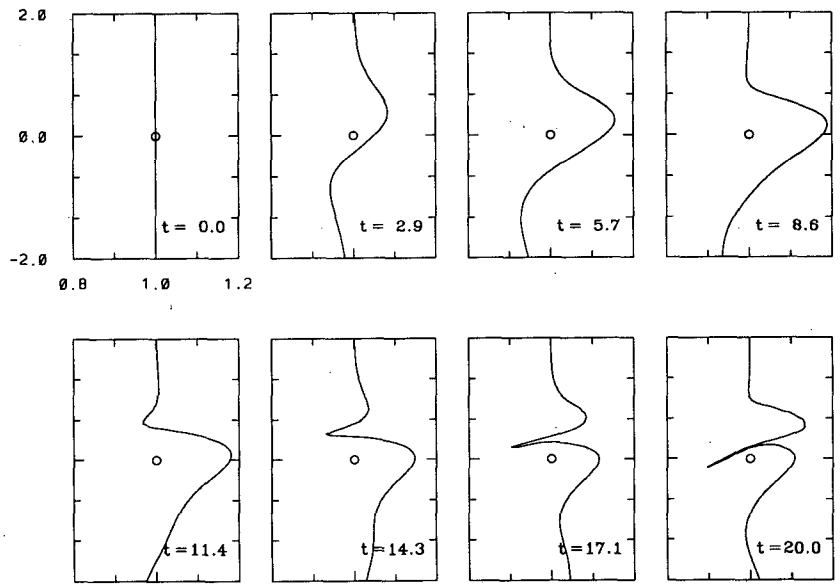

FIG. 2b. As in (a) but $h_0 = 0.2$.

section of the front near the topography rotates in a clockwise direction and a disturbance is formed. The lower part of this disturbance is advected by the basic flow, giving rise to a wave moving downstream in the negative y direction. This is clearly seen by noting how the lower end of the contour, initially at $(x, y) = (1, -2)$, moves through the integration interval, as opposed to the upper point $(x, y) = (1, 2)$, which remains fixed for all time. The primary disturbance, which is trapped by the topographic feature, reaches an amplitude of about 0.1 at $t = 8.6$ and then decreases to about 0.05 at $t = 17.1$. The integration is stopped at $t = 20$ when the amplitude has begun to increase again, but the waves have shown no sign of steepening within this time interval. The formation of another traveling disturbance is clearly seen downstream of the topographic center.

Figure 2b shows the evolution for $h_0 = 0.2$. The initial evolution up to $t = 8.6$ is qualitatively similar to Fig. 2a, but now the amplitudes of the waves formed, both the trapped and the moving disturbance, increase to almost twice the values of the previous case. For $t = 14.3$, however, a qualitative change occurs. The trapped wave steepens and at $t = 17.1$ it "breaks," reaching an amplitude of about 0.1. Here breaking is defined to be the onset of filamentation. At $t = 20$ the two sections of the contour touch one another. Grimshaw and Yi (1991, 1992) showed that the presence of a critical level is responsible for the filamentation process. A critical level is here defined as a value of $x = x_c$, such that the phase speed c of a linear wave is equal to the speed of the basic flow $v_0(x_c)$; that is,

$$v_0(x_c) - c = 0. \tag{4.2}$$

A linearized wave analysis is performed in appendix B and shows that in our case a critical level is present for

$$x_c \approx 0.86, \tag{4.3}$$

for the parameter values of Fig. 2. This is in good agreement with the observed filament at $t = 17.1$. For $h_0 = 0.1$ the wave amplitude is not large enough to reach the critical level and hence filamentation does not occur. As the topographic amplitude increases, the primary wave amplitude also increases until we reach a "critical" value of h_0 (between 0.1 and 0.2 in our case), where the wave reaches the critical level and filamentation occurs from there on.

Figures 3a,b and 4a,b show the evolution for $h_0 = 0.6$, 1.0, 1.5, and 2.5, respectively. The x-axis range has been changed to $0 < x < 2$ to allow for an increased wave amplitude and the y-axis range has been increased to $-9 < x < 3$ to observe the evolution of the secondary traveling disturbance with more clarity. When $h_0 = 0.6$ the trapped wave amplitude reaches a value of about 0.5 at $t = 8.6$ and the length of the filament has increased considerably at $t = 20$ compared to $h_0 = 0.2$. The behavior for $h_0 = 1.0$ (Fig. 3b) is qualitatively similar to $h_0 = 0.6$. The wave amplitudes, however, have increased by about 50%, the trapped wave amplitude now reaching a maximum of about 0.8 at $t = 8.6$ and the moving disturbance a maximum of about 0.4. Although the amplitude of the secondary disturbance is large and it now reaches the critical level, its large "wavelength" does not allow it to steepen and hence breaking and filamentation do not occur.

Next, by increasing h_0 to 1.5 and 2.5 (Figs. 4a and 4b, respectively), the moving disturbance begins to show signs of steepening and reaches a maximum amplitude of about 0.6. When $h_0 = 2.5$ this wave breaks at $t = 8.6$ and a long filament near the coastline $x = 0$ is clearly visible. Its amplitude is not only large enough to reach the critical level, but also it has steepened sufficiently to allow breaking and filamentation to occur. This secondary filament is advected by the basic flow as opposed to the primary filament, which remains virtually trapped by the topographic feature. The structure of the trapped wave is also qualitatively different from the previous cases with its filament now forming downstream of the topographic center.

Increasing h_0 even further ($h_0 = 3.5$, 4.0 in Figs. 5a and 5b, respectively) yields yet another qualitative change. For $h_0 = 3.5$ there is now a clear tendency observed at $t = 5.7$ for the disturbance to wind around the topographic feature. The basic flow, however, overcomes this tendency and the disturbance is finally advected downstream. The amplitude of the stationary wave near the topography is now approximately 1.2. When $h_0 = 4.0$ (Fig. 5b), we again observe the tendency of the wave to rotate around the center. This time, however, although a section of the front is advected by the basic flow, a blob of oceanic fluid with potential vorticity $Q_0 = 0$ remains stationary between the coast and the topographic center. A balance has been reached between the tendency to rotate about the center and the tendency of advection by the basic flow. At $t = 12.1$ there is only a long filament joining the vortex with the rest of the front and by $t = 17$, the vortex clearly remains stationary well inside the coastal fluid of vorticity $Q_1 = 1$.

For $h_0 = 5$ (Fig. 6a) the contour winds around the center forming a trapped eddy with substantial internal mixing. By time $t = 8$ the eddy has clearly detached, remaining linked to the main contour by a long thin filament that now touches the coastline. Increasing to $h_0 = 6$ (Fig. 6b) has the effect of increasing the size of the eddy as well as the amount of internal mixing. At $t = 8$ the eddy becomes distorted by the presence of the coastline and the basic flow. The number of points on the contour reached 1200 in this case and the integration had to be stopped. It is quite evident that to continue the integration for longer periods of time a contour surgery algorithm needs to be used to remove the long filaments and other small-scale structure present in the system.

b. Varying ξ

Here we fix $h_0 = 1$ (leaving $Q_0 = 0$ and $\Delta Q = 1$) and vary the topographic parameter ξ. According to

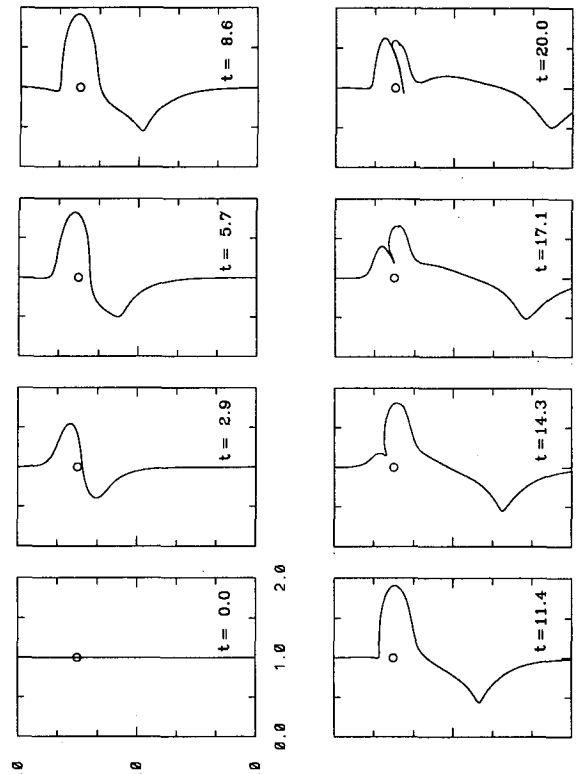

FIG. 3a. Evolution for $h_0 = 0.6$.

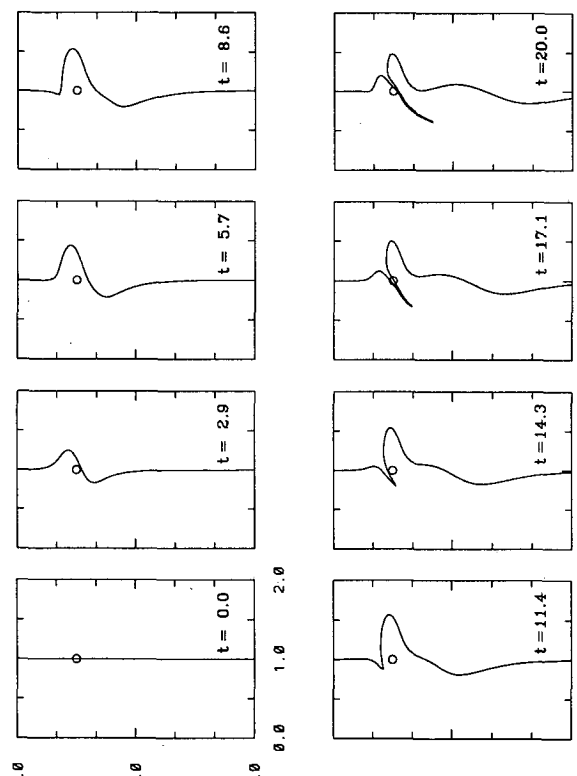

FIG. 3b. $h_0 = 1.0$. All other parameters as in Fig. 2.

FIG. 4a. Evolution for $h_0 = 1.5$.

FIG. 4b. $h_0 = 2.5$.

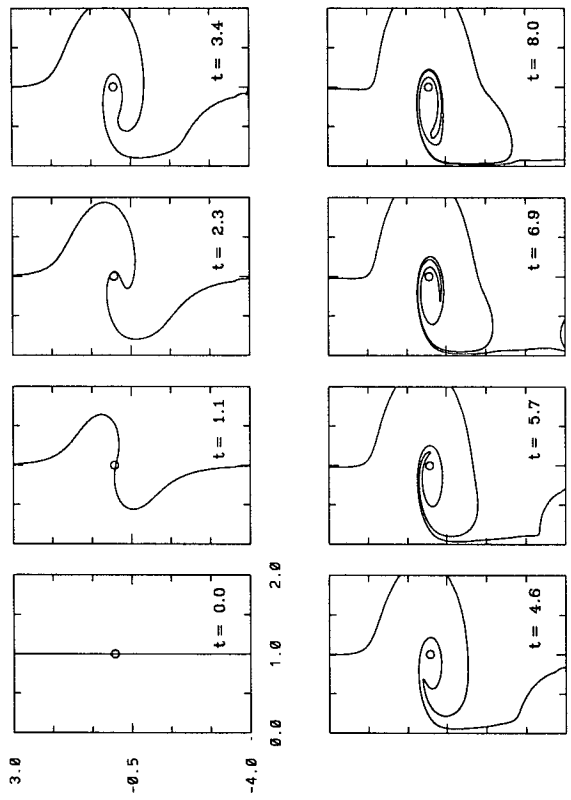

FIG. 5a. Evolution for $h_0 = 3.5$.

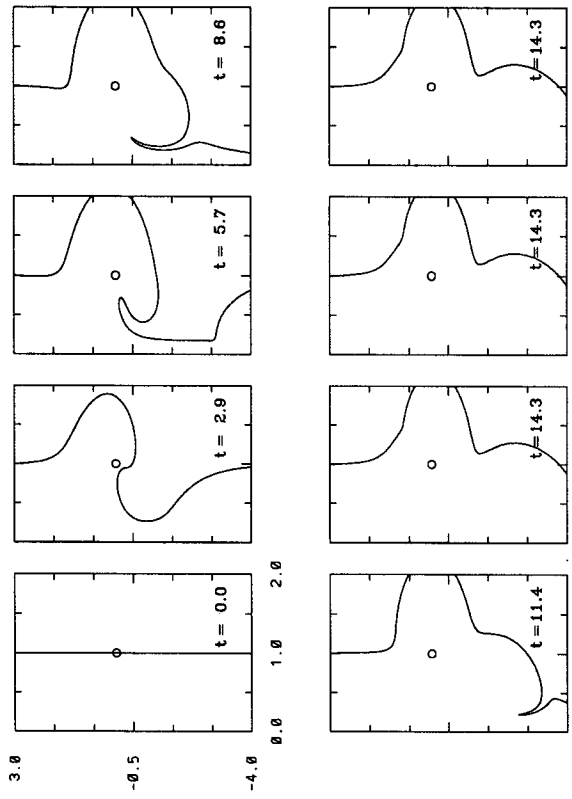

FIG. 5b. $h_0 = 4.0$.

FIG. 6a. Evolution for $h_0 = 5.0$.

FIG. 6b. $h_0 = 6.0$.

the linearized analysis in appendix B, the site of filamentation is a function of ξ in the manner given by Eq. (B.10). For $\xi = 0.5$ (Fig. 7a), the critical level is $x_c \approx 0.76$ and is therefore moved further away from the topographic center. However, since $\xi^{-1/2}$ is the half-width of the topography, smaller values of ξ increase the width of the bump, which has the effect of increasing the amplitude and wavelength of the wave at the initial stages of evolution of the front (e.g., $t = 4.3$). Hence, although the critical level is now farther away, the larger amplitudes produced mean that the critical level is reached by the disturbance and filamentation still occurs.

For $\xi = 4$ (Fig. 7b) we have a narrow bump and the amplitude generated at $t = 4.3$ is much smaller. However, now the critical level $x_c \approx 0.88$ has moved closer to the center and hence filamentation also occurs. This explains the similar qualitative behavior obtained for different values of ξ (cf. Fig. 3b, where $\xi = 3$).

c. *Varying Q_0*

We now fix the parameters $\Delta Q = 1$, $h_0 = 1$, $\xi = 3$, and study the effect of varying the ocean potential vorticity Q_0. Figures 8a,b show the evolution to $t = 15$ when $Q_0 = 0.1, 0.2$, respectively. A positive value of potential vorticity Q_0 has the effect of inhibiting wave breaking and the formation of a filament. Note that a positive value of Q_0 implies that $v_0(l) < 0$ [see (2.7a)], and hence the advective effect of the basic flow in the negative y direction is enhanced as Q_0 increases.

Figure 9a shows the case $Q_0 = -0.1$ so that now $v_0(l) > 0$. The presence of negative potential vorticity for $x > l$ produces a result qualitatively similar to Fig. 3b (where all other parameters are the same, except $Q_0 = 0$). The main difference is that the filament produced now is wider near the topographic center. Changing Q_0 to -0.2 (Fig. 9b) gives an evolution similar to Fig. 9a up to $t = 17.1$. At $t = 21.4$, however, a large vortex begins to form and at $t = 30$ it detaches, giving rise to the formation of an eddy of potential vorticity Q_1 to the right of the topographic center. The thick filament of vorticity Q_0 now has a more complicated wavy structure compared to the corresponding filament in Fig. 9a.

Figure 9c shows the case $Q_0 = -0.3$. Here again a large vortex is formed at $t = 30$. The filament, however, does not continue increasing in length downstream but points away from the coastline and remains upstream of the topography. Finally, changing Q_0 to -0.4 (Fig. 9d) produces another qualitative change in the evolution after about $t = 14.3$. The initial stages remain similar to the three previous figures; however, now there is no sign of filamentation and no vortex is formed up to $t = 25$. In fact the disturbance does not steepen or break and shows little signs of change for $t = 17.9$, 21.4, and 25.0. The reason for this is the strong effect of the basic flow in the positive y direction. It is clear from (2.7a) that when $Q_0 < 0$ then $v_0 > 0$ both inshore and offshore of the potential vorticity front.

Our results indicate that filamentation is sensitive to the sign and strength of the basic flow. However, they have been obtained for a particular value of the topographic amplitude of $h_0 = 1$. Based on the previous simulations, it is conceivable that larger h_0 will increase steepening of the front even for large values of Q_0 leading to filamentation, but clearly more simulations are needed to confirm this point.

d. *Varying l*

We now fix the parameters $\Delta Q = 1$, $Q_0 = 0$, $h_0 = 1$, and $\xi = 3$ and vary the position l of the undisturbed front. Figure 10a shows the evolution for the case $l = 1.2$. Increasing l has decreased the tendency of wave breaking and although the evolution is qualitatively similar to Fig. 3b, the length of the filament has now decreased considerably at $t = 20$. Increasing to $l = 1.3$ (Fig. 10b) has the effect of totally inhibiting wave breaking and filament formation. Increasing l even further (not shown here) has the effect of decreasing the amplitude of the disturbance and consequently decreasing the possibility of wave breaking altogether.

Decreasing l, however, produces a different qualitative behavior. Figures 11a,b show the evolution for $l = 0.8, 0.6$, respectively. Comparing these two cases, it is apparent that there is now a clear tendency for the front to evolve into a disturbance of small width and large amplitude. These are the conditions found by Pratt and Stern (1986) that lead to vortex formation and eddy detachment. It is conceivable that extending the integrations further will indeed show that kind of behavior. However, decreasing l even further to 0.5 (Fig. 11c) shows that at $t = 20$ the two sections of the front over the topographic center are now very close together and that a vortex of potential vorticity Q_1 is about to form. Decreasing l to 0.4 in Fig. 11d clearly shows that at $t = 20$ the eddy is about to detach to the right of the topographic feature. The combined effects of trapping by the topography and advection by the basic flow produce a small width, large amplitude disturbance, which leads to the formation of a lobe of potential vorticity Q_1 and subsequent eddy detachment.

5. Summary

A simple quasigeostrophic model has been used to study the topographic forcing of fully nonlinear waves on an interface separating two regions of constant potential vorticity. Different qualitative behaviors were found by varying the amplitude h_0 of the topographic forcing and keeping all other parameters fixed. In particular, the disturbances increased in amplitude and complexity as h_0 was increased. The three main features of the nonlinear behavior are 1) the filamentation process, whose initiation is caused by the presence of a

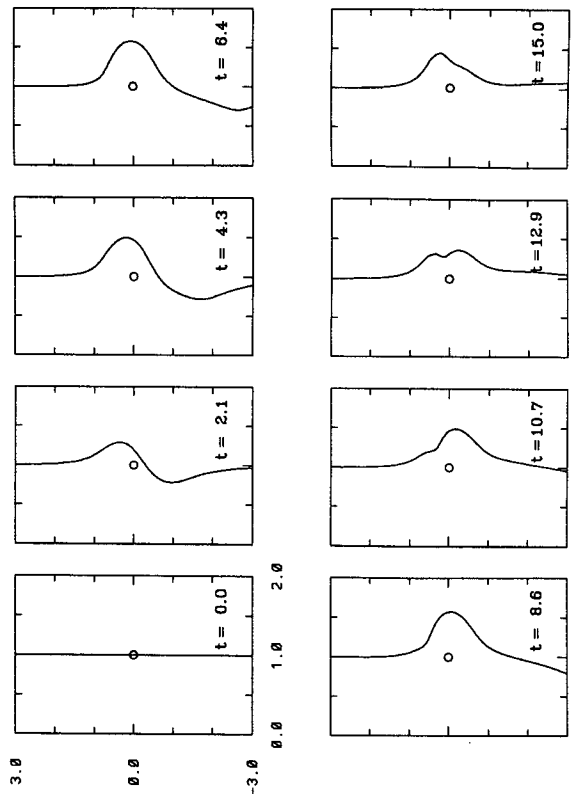

FIG. 7a. Evolution for $Q_0 = 0$, $\Delta Q = 1$, $h_0 = 1$, $l = 1$, and $\xi = 0.5$.

FIG. 8a. Evolution for $\Delta Q = 1$, $h_0 = 1$, $\xi = 3$, $l = 1$, and $Q_0 = 0.1$.

FIG. 7b. $\xi = 4$. All other parameters as in (a).

FIG. 8b. $Q_0 = 0.2$. All other parameters as Fig. 8a.

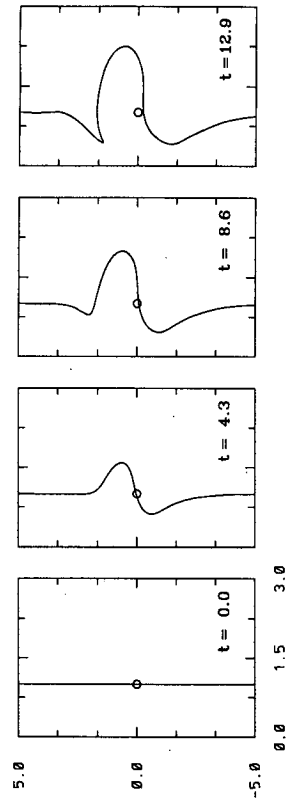

FIG. 9a. Evolution for $Q_0 = -0.1$.

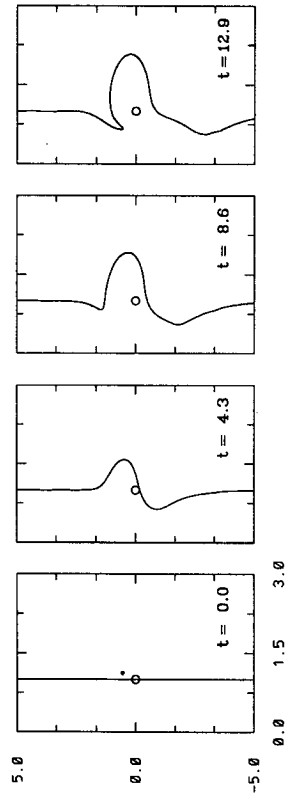

FIG. 9b. Evolution for $Q_0 = -0.2$.

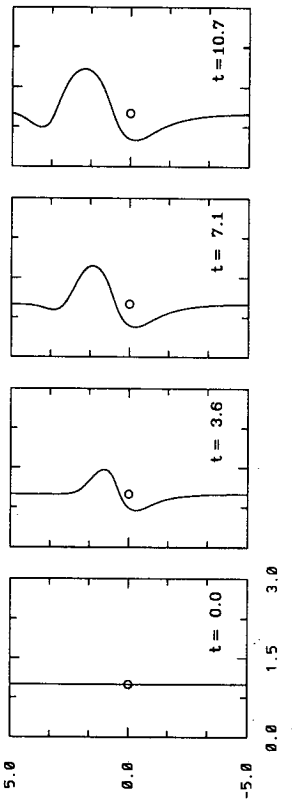

FIG. 9d. Evolution for $Q_0 = -0.4$.

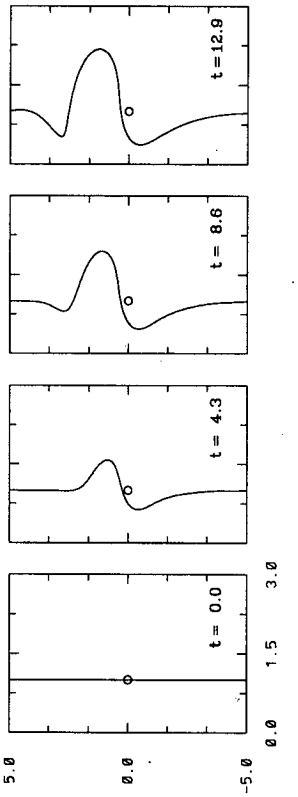

FIG. 9c. Evolution for $Q_0 = -0.3$.

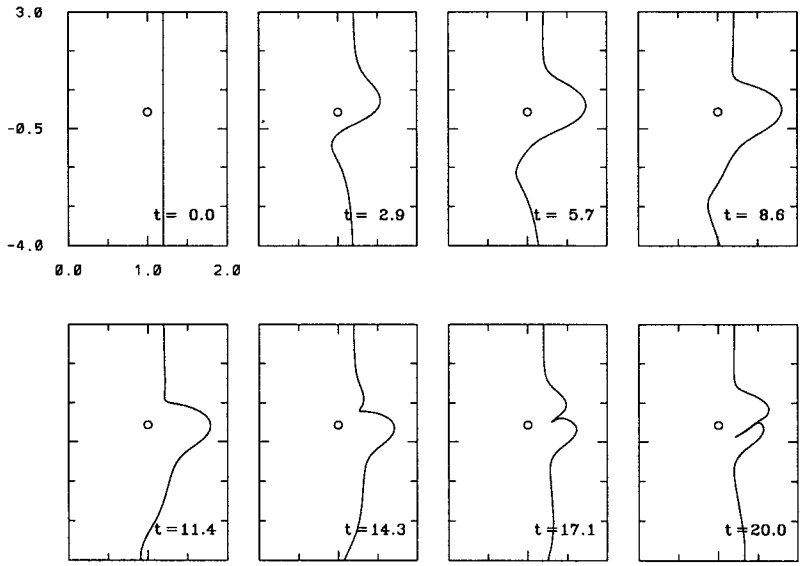

FIG. 10a. Evolution for $Q_0 = 0$, $\Delta Q = 1$, $h_0 = 1$, $\xi = 3$, and $l = 1.2$.

critical level, 2) the formation of a trapped eddy with considerable internal mixing of the two fluids of potential vorticities Q_0 and Q_1 (Figs. 6a–c), and 3) the formation of eddies of potential vorticity Q_1 on the ocean side of the topographic feature (Figs. 9b,c and 12c,d). In general, the combination of a potential vorticity front and a topographic feature of sufficient amplitude can produce large eddies in the coastal ocean. Our results show that filamentation is sensitive to the sign and strength of the basic flow for a fixed value of the topographic amplitude.

It must be emphasized that the basic flow (2.7b) is linearly stable for all parameter values and that the structures present in the system are formed entirely due to nonlinear dynamical processes. It is interesting to compare this behavior with, for example, the results of Pratt and Pedlosky (1991). They use an unstable basic flow to allow wave growth to occur up to a certain amplitude and then they stabilize the linear basic state and show that the subsequent evolution and growth of the waves are also entirely due to nonlinear behavior. Grimshaw and Yi (1991, 1992) reached a similar con-

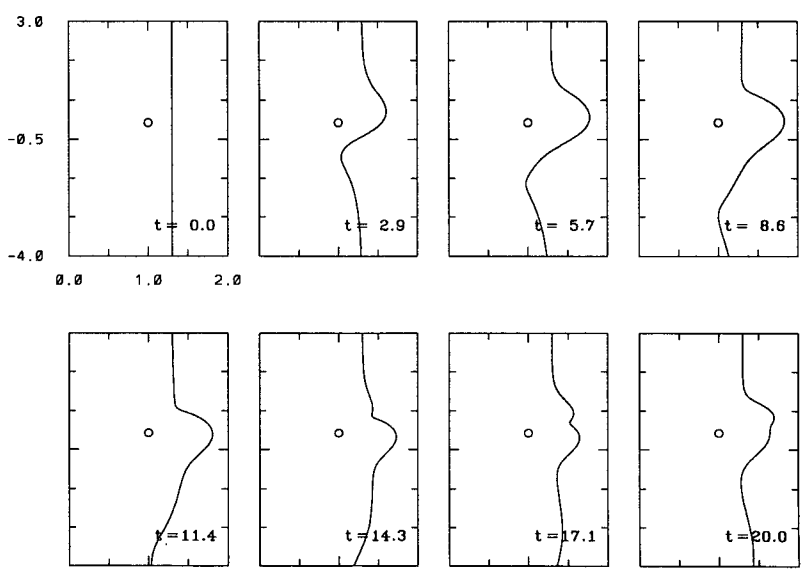

FIG. 10b. $l = 1.3$.

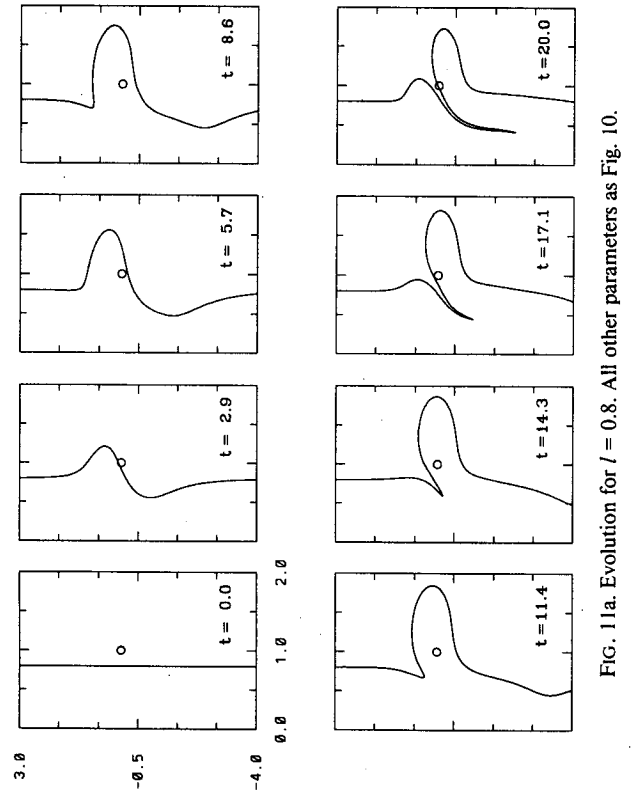

FIG. 11a. Evolution for $l = 0.8$. All other parameters as Fig. 10.

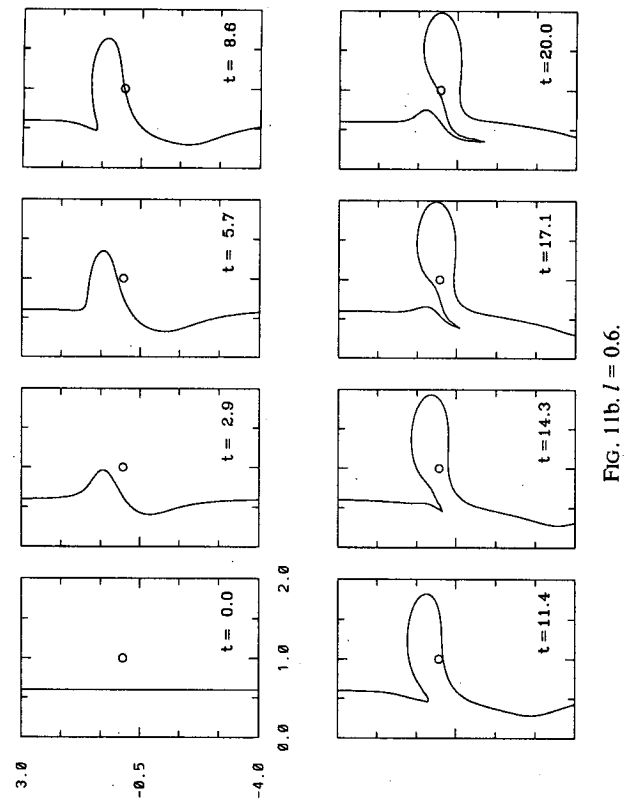

FIG. 11b. $l = 0.6$.

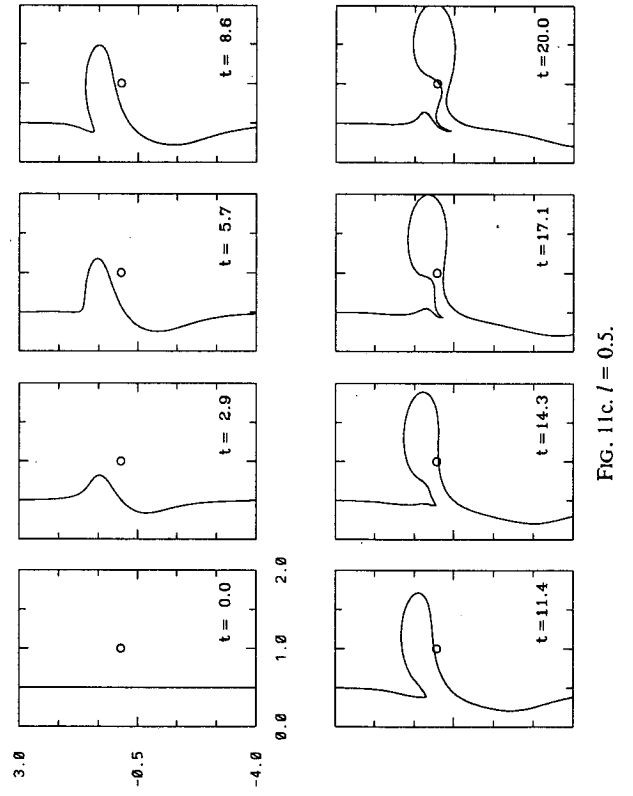

FIG. 11c. $l = 0.5$.

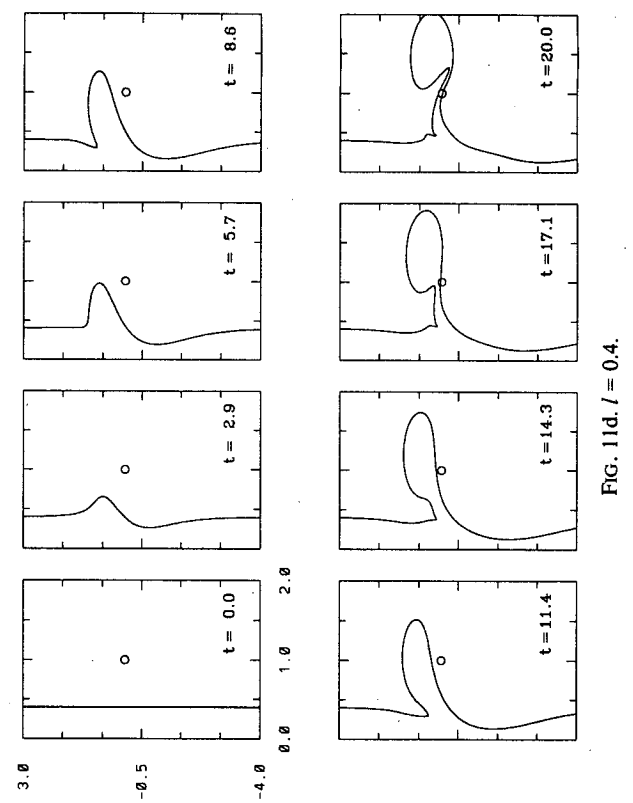

FIG. 11d. $l = 0.4$.

clusion on their study of evolution over a topographic slope with a stable basic flow. In summary, it is clear that filamentation, vortex formation, and subsequent eddy detachment are robust features of the nonlinear systems describing the formation and evolution of coastal mesoscale phenomena.

The simple model used here does not include the full effects of stratification and the introduction of an active upper layer is a logical extension of the system. This would also allow the study of the combined effects of both topographic forcing and instability of the basic state. These problems are currently under investigation. Finally, we emphasize that the quasigeostrophic model is only valid for topographic amplitudes of the order of the small Rossby number Ro. The introduction of larger topographic amplitudes than this model allows will be the subject of future studies.

APPENDIX A

Simplification of the Integrals A_1 and A_2

Defining

$$I(x, y) = -\int_{-\infty}^{\infty}\int_{-\infty}^{\infty} h(x', y')G(R)dx'dy', \quad \text{(A.1a)}$$

where

$$R = [(x - x')^2 + (y - y')^2]^{1/2}, \quad \text{(A.1b)}$$

we have

$$A_1(x, y) = -\frac{\partial}{\partial y}[I(x, y) - I(-x, y)]$$

$$= -\frac{\partial}{\partial y} I(x, y) + \frac{\partial}{\partial y} I(-x, y) \quad \text{(A.2a)}$$

$$A_2(x, y) = \frac{\partial}{\partial x}[I(x, y) - I(-x, y)]$$

$$= \frac{\partial}{\partial x} I(x, y) + \frac{\partial}{\partial(-x)} I(-x, y). \quad \text{(A.2b)}$$

Let

$$X' = x' - x = \lambda\cos\theta, \quad Y' = y' - y = \lambda\sin\theta,$$

$$X = x - \bar{x}_0 = A\cos\phi, \quad Y = y - \bar{y}_0 = A\sin\phi,$$

$$\lambda^2 \equiv R^2 = (x - x')^2 + (y - y')^2,$$

$$A^2 = (x - \bar{x}_0)^2 + (y - \bar{y}_0)^2.$$

Then using (2.10) and (3.6) we can write

$$I = \frac{h_0}{2\pi}\int_0^{2\pi}\int_0^{\infty} \exp[-\xi(\lambda^2 + 2\lambda A \times \cos(\theta - \phi) + A^2)]K_0(\lambda)\lambda d\lambda d\theta. \quad \text{(A.3)}$$

Hence

$$I = h_0 e^{-\xi A^2}\int_0^{\infty} K_0(\lambda)e^{-\xi\lambda^2} \times \left\{\frac{1}{2\pi}\int_0^{2\pi} e^{-2\xi\lambda A\cos\theta}d\theta\right\}\lambda d\lambda = h_0 e^{-\xi A^2} \times \int_0^{\infty} K_0(\lambda)e^{-\xi\lambda^2} I_0(2\xi\lambda A)\lambda d\lambda, \quad \text{(A.4)}$$

where $I_0(\cdot)$ is the modified Bessel function of the first kind. Then

$$\frac{\partial I}{\partial y} = \frac{\partial I}{\partial Y} = \frac{Y}{A}\frac{\partial I}{\partial A} \quad \text{(A.5a)}$$

$$\frac{\partial I}{\partial x} = \frac{\partial I}{\partial X} = \frac{X}{A}\frac{\partial I}{\partial A}. \quad \text{(A.5b)}$$

Now

$$\frac{\partial I}{\partial A} = 2\xi h_0 e^{-\xi A^2}\int_0^{\infty} e^{-\xi\lambda^2} K_0(\lambda)I_1(2\xi\lambda A)\lambda^2 d\lambda - 2\xi A h_0 e^{-\xi A^2}\int_0^{\infty} e^{-\xi\lambda^2} K_0(\lambda)I_0(2\xi\lambda A)\lambda d\lambda$$

$$= 2\xi h_0 e^{-\xi A^2}\int_0^{\infty} e^{-\xi\lambda^2} K_0(\lambda)I_1(2\xi\lambda A)\lambda^2 d\lambda + \frac{h_0}{2\xi A}e^{-\xi A^2}\int_0^{\infty} e^{-\xi\lambda^2}(2\xi A\lambda)I_1(2\xi A\lambda)\{K_0'(\lambda) - 2\xi\lambda K_0(\lambda)\}d\lambda$$

$$= -h_0 e^{-\xi A^2}\int_0^{\infty} e^{-\xi\lambda^2} I_1(2\xi\lambda A)K_1(\lambda)\lambda d\lambda. \quad \text{(A.6)}$$

Substituting (A.6) into (A.5) and using (A.2) we finally obtain (3.7a) and (3.7b). We note that $\lambda K_1(\lambda)$ is finite as $\lambda \to 0$ and therefore the integrand is finite as $\lambda \to 0$.

APPENDIX B

Linearized Wave Analysis

The linearized wave equation in the absence of topographic forcing [i.e., $h(x, y) = 0$] is

$$\nabla^2\phi - \phi = 0, \quad x \neq l, \quad \text{(B.1)}$$

with boundary conditions given by the kinematic condition

$$L_t + v_0 L_y = -\phi_y \quad \text{at} \quad x = l, \quad \text{(B.2)}$$

where $v_0(l) = -Q_0$ [see (2.7a)] and

$$[\phi]_-^+ = 0 \quad \text{(B.3a)}$$

$$[\phi_x]_-^+ = \Delta Q(L - l), \quad \text{(B.3b)}$$

across $x = l$.

Assuming a y, t dependence of the form

$$(\phi, L) = (\hat{\phi}(x), \hat{L})e^{ik(y-ct)}, \tag{B.4}$$

substitution into (B.1) and satisfying (B.3a) gives

$$\hat{\phi} = \begin{cases} \phi_0 e^{-\sqrt{k^2+1}(x-l)}, & \text{for} \quad x > l \\ \phi_0 \dfrac{\sinh\sqrt{k^2+1}\,x}{\sinh\sqrt{k^2+1}\,l}, & \text{for} \quad 0 < x < l. \end{cases} \tag{B.5}$$

Similarly, substituting into (B.2) and using (B.4) gives

$$(\hat{L} - l)[v_0(l) - c] = -\phi_0.$$

Applying the boundary condition (B.3b) then yields

$$c - v_0(l) = -\frac{\Delta Q}{2\sqrt{k^2+1}}\{1 - e^{-2\sqrt{k^2+1}l}\}. \tag{B.6}$$

This shows in particular that the basic flow is linearly stable.

Now critical levels occur where $v_0(x_c) = c$ or

$$v_0(x_c) - v_0(l) = -\frac{\Delta Q}{2\sqrt{k^2+1}}\{1 - e^{-2\sqrt{k^2+1}l}\}. \tag{B.7}$$

But from (2.7a) we have that

$$v_0(x_c) = -Q_0 e^{-(x_c-l)} + \Delta Q \sinh(x_c - l)H(l - x_c) \tag{B.8a}$$

and

$$v_{0x}(l) = \begin{cases} Q_0, & \text{for} \quad x_c > l \\ Q_1, & \text{for} \quad x_c < l. \end{cases} \tag{B.8b}$$

Hence, using a Taylor expansion we may approximate

$$v_0(x_c) - v_0(l) \approx \begin{cases} Q_0(x_c - l), & \text{for} \quad x_c > l \\ Q_1(x_c - l), & \text{for} \quad x_c < l. \end{cases} \tag{B.9}$$

Finally, using (B.9) and (B.7) we obtain

$$Q_0(x_c - l) \approx -\frac{\Delta Q}{2\sqrt{k^2+1}}\{1 - e^{-2\sqrt{k^2+1}l}\}, \quad \text{for} \quad x_c > l, \tag{B.10a}$$

which requires $Q_0 \Delta Q < 0$. Similarly

$$Q_1(x_c - l) \approx -\frac{\Delta Q}{2\sqrt{k^2+1}}\{1 - e^{-2\sqrt{k^2+1}l}\}, \quad \text{for} \quad x_c < l \tag{B.10b}$$

and this requires that $Q_1 \Delta Q > 0$. To use these formulas we must choose an appropriate value for the wavenumber k. Assuming that this is provided by the topographic forcing, we take the Fourier transform of $h(x, y)$ in (3.6) with respect to y and deduce that an approximate value for k is $2\sqrt{\xi}$. For the parameter values of Fig. 2 ($Q_0 = 0$, $\Delta Q = 1$, $\xi = 3$, $l = 1$) the critical level is given by (B10.b) with $k \approx 3.5$. Hence $l - x_c \approx 0.14$ or $x_c \approx 0.86$.

REFERENCES

Brink, K. H., and T. J. Cowles, 1991: The Coastal Transition Zone Program. *J. Geophys. Res.*, **96,** 14 637–14 647.

Dritschel, D. G., 1989: Contour dynamics and contour surgery: Numerical algorithms for extended, high-resolution modeling of vortex dynamics in two-dimensional, inviscid, incompressible flows. *Comput. Phys. Rep.*, **10,** 77–146.

Griffiths, R. W., and A. F. Pearce, 1985: Instability and eddy pairs on the Leeuwin Current south of Australia. *Deep-Sea Res.*, **32,** 1511–1534.

Grimshaw, R., and Z. Yi, 1991: Evolution of a potential vorticity front over a topographic slope. *J. Phys. Oceanogr.*, **21,** 1240–1255.

——, and ——, 1992: Processes leading to filamentation of a potential vorticity interface over a topographic slope. *Breaking Waves, Proc. IUTAM Symp.*, Sydney, M. L. Banner and R. H. J. Grimshaw, Eds., Springer, 357–366.

Haidvogel, D. B., A. Beckmann, and K. S. Hedstrom, 1991: Dynamical simulations of filament formation and evolution in the coastal transition zone. *J. Geophys. Res.*, **96,** 15 017–15 040.

Huyer, A., and P. M. Kosro, 1987: Mesoscale survey over the shelf and slope in the upwelling region near Pt. Arena, California. *J. Geophys. Res.*, **92,** 1655–1681.

Jacobs, P. A., and D. I. Pullin, 1989: Multiple-contour-dynamic simulation of eddy scales in the plane shear layer. *J. Fluid Mech.*, **199,** 89–124.

Kosro, P. M., 1987: Structure of the coastal current field off northern California during the Coastal Ocean Dynamics Experiment. *J. Geophys. Res.*, **92,** 1637–1654.

Narimousa, S., and T. Maxworthy, 1989: Application of a laboratory model to the interpretation of satellite and field observations of coastal upwelling. *Dyn. Atmos. Oceans*, **13,** 1–46.

Pratt, L. J., and M. E. Stern, 1986: Dynamics of potential vorticity fronts and eddy detachment. *J. Phys. Oceanogr.*, **16,** 1101–1120.

——, and J. Pedlosky, 1991: Linear and nonlinear barotropic instability of geostrophic shear layers. *J. Fluid Mech.*, **224,** 49–76.

Pullin, D. I., and P. A. Jacobs, 1986: Inviscid evolution of stretched vortex arrays. *J. Fluid Mech.*, **171,** 377–406.

Send, U., 1989: Vorticity and instability during flow reversals on the continental shelf. *J. Phys. Oceanogr.*, **19,** 1620–1633.